Direct Printing of Micropatterned Plasmonic Substrates of Size-controlled Gold Nanoparticles by Precision Photoreduction

Yangxi Zhang[1], Zengtian Liang[1], A. Ping Zhang[1]* and Hwa-Yaw Tam[1]

[1]Photonics Research Center, Department of Electrical Engineering, The Hong Kong Polytechnic University, Hung Hom, Hong Kong SAR, China

*Email address: azhang@polyu.edu.hk

Keywords: plasmonic substrate, gold nanoparticle, optical printing, precision photoreduction

Abstract: Although the extraordinary optical property of gold nanoparticles (AuNPs) has been known for a long time, the anticipated applications of AuNPs in plasmonically enhanced substrates and photonic microdevices are still under development. In this paper, we present a method for the direct printing of micrometer-scale patterns of size-controlled AuNPs for plasmonic substrates and microsensor development. Using in-house digital UV lithography, a precision photoreduction technology is developed for light-controlled growth of AuNPs to create micrometer-scale micropatterns on a titanium dioxide photocatalytic layer. The titanium dioxide thin layer not only enables a photocatalytic reduction process for high-precision printing of size-controlled AuNPs in an additive manner, but also introduces a Fano resonance that can sharpen spectral width of localized surface plasmon resonance peak and increase its peak-to-valley value. This printing technology can be used to cost-effectively fabricate size-scalable micropatterned plasmonic substrates of size-controlled AuNPs and thus offers new opportunities to develop various types of miniature plasmonic devices ranging from plasmonic biochemical sensors to plasmonically enhanced photothermal and photovoltaic microdevices.

1

The gold nanoparticle (AuNP) is a historical nanomaterial with novel optical and chemical properties that have aroused wide interest for over one hundred years. Since Michael Faraday's work on colloidal AuNPs, the distinct characteristics of AuNPs, including its unusual size- and shape-dependent optical responses, high surface-area-to-volume ratio, high chemical stability, and flexible surface modification abilities, have attracted great attention and extensive studies[1,2]. Notably, when AuNPs are irradiated by light, the conduction electrons of AuNPs exhibit collective oscillations known as localized surface plasmon resonance (LSPR)[3]. LSPR lends AuNPs certain remarkable optical characteristics, such as selective absorption and scattering spectra and a greatly enhanced local electromagnetic field[4]. Because of these unique competences, AuNPs have shown promise in many applications, such as photonic devices and meta-materials[5,6], organic and biomolecule sensing[7], drug/gene/protein delivery[8], plasmonic photothermal therapy[9], storage systems[10], plasmonic solar cells[11], and plasmonic photocatalysis[12].

To prepare AuNPs with a controlled size and morphology on a large scale, one can use chemical synthesis[13-15], gamma ray-assisted synthesis[16], photochemically assisted synthesis[17,18], ultrasonically assisted synthesis[19], in-water laser ablation of gold[20, 21], and biosynthesis[22, 23]. However, if the AuNPs synthesized in solution are used to fabricate micropatterned plasmonic devices and sensors, additional elaborate processes, such as inkjet printing and nanoimprinting[24-26], have to be further applied to deposit such AuNPs on a substrate (commonly referred to a plasmonic AuNP substrate). Moreover, one of the growing demands involves fabrication of micropatterns of AuNPs that enable the integration of multiple size-varied AuNPs for different purposes in photonic microsystems, such as lab-on-chip devices. To meet such a demand, electron-beam lithography (EBL) and EBL-based nanoimprinting have been used to precisely fabricate plasmonic nanostructures of AuNPs with control over size and shape for various applications, such as plasmonic metamaterials and

2

plasmonic color generation[27-29]. However, methods based on EBL are commonly costly and have low-throughput problem due to the use of expensive equipment and the single-spot scanning manner. Similar problems exist in pulsed or continuous-wave laser-based direct writing methods [30,31]. Deposition methods such as electrodeposition[32], sputtering[33] and evaporation/heat treatment[34] can be used to rapidly prepare plasmonic substrates of AuNPs, but these methods lack the ability to pattern the AuNPs at the microscale and thus require a further lithography process to achieve micropatterning of AuNPs. Therefore, direct and rapid fabrication of micrometer-scale patterns of size-controlled or size-varying AuNPs remains as a challenge to unlocking the great potential of AuNPs for miniature plasmonic substrates and device applications.

Recently, we developed a precision photoreduction technology for fabrication of silver-nanoparticle micropatterns and demonstrated their application on plasmonic color generation[35]. In this paper, we further develop this precision photoreduction technology to fabricate micropatterns of size-controlled AuNPs so as to exploit the advantages of AuNPs, such as special localized surface-plasmon resonance frequency range, facile surface-modification ability and low toxicity and excellent stability, for biosensing and plasmonically-enhanced applications. Dynamic ultraviolet (UV) light patterns are used to initiate, sustain and halt photocatalytic reduction of AuNPs from gold salt solution on a titanium dioxide (TiO_2)-capped quartz substrate. The photoreduction process is spatially and temporally regulated by mask-less UV exposure technology, so-called precision photoreduction, to directly print micropatterns of AuNPs with a controlled size. Experiments show that such a precision photoreduction technology for AuNPs can rapidly print high-resolution micropatterns of size-varying AuNPs. Additionally, the fabricated AuNPs-TiO_2-quatrz structure exhibited a Fano resonance. The figure of merit of the localized surface-plasmon resonance (LSPR) peak of the

plasmonic substrate is experimentally improved by enhancing the surface smoothness of the AuNPs via thermal treatment.

Using an in-house digital UV lithography system, dynamic optical exposure technology is utilized applied to programmatically customize the exposure dose and exposure location for size control and patterning, respectively, as shown in **Figure 1a**. An UV-grade spatial light modulator, i.e., digital micromirror device (DMD), is used to convert the uniform light beam from a 365-nm UV source to generate an UV pattern with a million pixels. After passing through an optical reduction-projection lens, the light pattern is projected upon the target substrate to initiate and regulate the photoreduction process. With pulse width modulation, the grayscale exposure technique is adopted to enable high-speed switch on/off light switching for precise control of the exposure doses so as to precisely customize the particle size at the nanometer scale. A high-precision motorized stage integrated within the optical exposure system enables the stitching of small UV patterns to fabricate larger-area plasmonic substrates.

To print high-resolution micropatterns of AuNPs on a substrate and suppress side reactions, a precision photoreduction technology based on the photocatalytic reduction reaction upon a thin TiO_2 layer is established. TiO_2 has a wide bandgap and can efficiently absorb UV light to generate photoelectrons, which can enable to preferentially reduce metal ions on the surface of the TiO_2 layer. Moreover, rather than the widely used tetrachloride gold (III) ion ($AuCl_4^-$), who which has a strong oxidizing ability, whose reduction potential is of +0.93V ($AuCl_4^-/Au(s)$), and thus can absorb UV light to directly oxidize various reducing agents under UV light in solution even without a photocatalyst, the gold(I) thiourea complex ion ($Au(SC(NH_2)_2)_2^+$) with a relatively lower reduction potential ($Au(SC(NH_2)_2)_2^+/Au(s)$, +0.38V) and less absorption to 365 nm UV light is used to achieve high-resolution precision photoreduction. The photocatalytic reduction reactions are described by **Equations 1 through 3** as follows:

$$TiO_2 \xrightarrow{h\nu} TiO_2(h^+) + e^- \tag{1}$$

$$Au(SC(NH_2)_2)_2^+ + e^- \longrightarrow Au(s) + 2SC(NH_2)_2 \tag{2}$$

$$C_6H_5O_7^{3-}(Citrate^{3-}) + 2TiO_2(h^+) \longrightarrow 2TiO_2 + C_5H_4O_5^{2-}(Acetonedicarboxylic^{2-}) + H^+ + CO_2 \uparrow \tag{3}$$
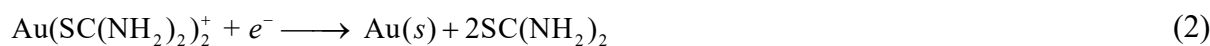
In the experiments, the TiO$_2$ photocatalytic layer is prepared by using the sol-gel method on a quartz plate, though other substrate with good UV transmittance and high temperature resistance, such as sapphire and glass, can also be used. Gold(I) thiourea complex ions are prepared by pouring thiourea into an acidified chloroauric acid solution with a quantitative reduction reaction and thereby adding an excess mount of sodium citrate to reduce the oxidized product of dithiocarbamate. Dithiocarbamate is eliminated from the solution to avoid oxidization of gold(s) back to gold (I) ions during the growth of the AuNPs. Potassium sodium tartrate is finally added as an auxiliary complexing agent. **Figure S1** shows a stability comparison of stability between the tetrachloride gold (III) ion and gold(I) thiourea complex ion solutions. After irradiation of 250 J/cm^2 by a UV source at 365 nm, the tetrachloride gold (III) ion solutions mixed with sodium citrate become purple-red and opaque in color, which indicates the creation of AuNPs by the UV irradiation, while the gold(I) thiourea complex ion solution keeps remains clear and colorless, which indicates its good UV-resistancet ability.

Thermal treatment has been widely used to reshape and improve the degree of crystallinity of AuNPs[36, 37]. In our experiments, a thermal treatment process (2 h @ 300 ºC, in air) is adopted to improve the surface smoothness and crystallinity of the directly printed AuNPs. Moreover, the process can remove the thiourea monolayer on the surface of AuNPs to supply a clean surface for future modification and applications. The process flow of light-controlled growth and thermal treatment of AuNPs is shown in Figure 1c.

Figure 2 shows images of the fabricated AuNP micropatterns printed on a titanium dioxide/quartz substrate under an illumination intensity of 1803 mw/cm^2. The exposure doses of the samples ranged from 180 to 541 J/cm^2, and all samples were thermally treated at 300 ºC

for 2 h. Figure 2a (i) and (ii) show the optical reflection-mode microscope images of AuNP micropatterns viewed from AuNP side and TiO$_2$-layer side, respectively. With the increase of exposure dose, the colors of the samples viewed from AuNP side vary from light aquamarine to dark salmon, while the colors of the samples viewed from TiO$_2$-layer side change from light lavender to dark turquoise. Notably, the sample printed with a high exposure dose (e.g., 541 J/cm^2) shows a red-toned color in the optical reflection-mode microscope images taken from the AuNP side and a complementary green-toned color in the image taken from TiO$_2$-layer side. Such a color change is one of the well-known features of AuNPs and can be traced back to the ancient Roman Lycurgus cup, the nanoparticles of which make its color shift from red to green under different illumination conditions[38]. The collection of all these colors are presented in Figure 2b. The dark-field microscopy images of the samples viewed from AuNP side display reddish color, as presented in **Figure S2**. Figure S3 shows the printed 2D grating of the AuNPs, and their diffraction pattern of which was generated using a 633 nm laser. The printing resolution is tested using a multiple-line pattern, as shown in Figure 2c. Due to proximity effect, the minimum linewidth achieved in the experiments is 3.64 μm (printed by using an optical pattern with the width of about 0.49 μm), which indicates the potential use of this printing technology in applications to high-resolution plasmonic microdevices.

Figure 3 shows the scanning-electron microscope (SEM) images of the AuNPs printed with different exposure doses and their corresponding reflection spectra taken from two sides of the micropatterns. With an increase in the exposure dose from 90 to 541 J/cm^2, the size of the fabricated AuNPs gradually increased and their distribution changed from sparse to dense. After thermal treatment for 2 h at 300 ºC, the surface of the nanoparticles becomes smoother, and the relatively smaller nanoparticles disappear. The reflection spectra of the fabricated plasmonic substrates of the AuNPs corresponding to Figure 3b are shown in Figure 3c. In the reflection spectra measured from the AuNPs side, one can see a clear spectral peak for which the

wavelength shifted from 577 nm to 626 nm with the increase in AuNP size. In the reflection spectra measured from TiO_2-layer side, one can observe a spectral dip with a dip wavelength that matches well with the peak wavelength in the reflection spectra measured from the AuNP side.

More detailed morphology information for the fabricated AuNPs is given in **Figure 4**. Figure 4a shows the high-magnification SEM images of the AuNPs before and after thermal treatment. Notably, in the presence of thiourea, many clusters of AuNPs, rather than Au particles, were formed when the exposure dose was relatively high. It may attribute to the complicated dynamic behaviors of AuNP growth kinetics. Initially, tiny AuNP seeds were randomly produced according to the random grain orientation of the polycrystalline TiO_2 layer. Thereafter, these AuNP seeds altered the movement path of newly photo-generated electrons, and the electrons that moved across small AuNPs reduced more gold(I) thiourea complex ions to form AuNP clusters. After thermal treatment, these tiny particles disappeared, and the surface of AuNPs became smoother. From the particle size distributions (see Figure 4b and Figure 4c), it can be observed that the average particle size of the AuNPs fabricated using a lower exposure dose (i.e., < 270 J/cm^2) became slightly smaller after thermal treatment, and the average diameter of the AuNPs fabricated using a higher exposure dose (i.e., >361 J/cm^2) became significantly larger after thermal treatment. As shown in Figure 4d, the expected value (EV) of the particle size of the AuNPs fabricated using an exposure dose of 541 J/cm^2 increased by 46.8% after thermal treatment, and its coefficient of variation (SD/EV) decreased by 37.7%. The phenomena can be attributed to the low melting point of the gold particles at the nanometer scale, which leads to a reshaping of small AuNPs from oblate spheroids to symmetrical spheres that is observed as a reduction of the particle size imaged from the vertical direction. For these relatively large AuNPs, tiny nanoparticles around the AuNPs might merge into a relatively large

7

nanoparticle during thermal treatment, which can explain the disappearance of the small particles and the reduction of variation after thermal treatment.

To understand the measured reflection spectra of the AuNPs-TiO$_2$-quartz structure, a numerical simulation based on the finite element method (COMSOL Multiphysics) was conducted and compared with the experimental results. **Figure 5a** shows the simulation model in which AuNPs are modelled as oblate particles according to the SEM image shown in **Figure S4** and the observation port is set to the AuNPs side to ensure that the model is consistent with the case of a plasmonic substructure for refractive index or bio-sensing. The oblate shape might result from attachment of AuNPs on the substrate during thermal treatment, which leads to oblate particles with a longer dimension in the horizontal plane than the height in the vertical direction.

Figure 5b shows a comparison of the measured and simulated reflection spectra of the AuNPs-TiO$_2$-quartz whose AuNPs were printed with the exposure dose of 361 J/cm^2. The size of particles was derived from the data given in Figure 4d. The numerical simulations revealed that the simulated reflection spectra matched well with the experimental results. Moreover, the influence of the substrates on the optical response of the entire AuNP-based structures was also evaluated by comparing the reflection spectra of the structures without and with different substrates. As shown in Figure 5b, the reflection spectra of AuNPs without a substrate or on a quartz substrate showed a symmetric spectral peak in the wavelength range from 500 to 700 nm, which can be attributed to the localized surface-plasmon resonance (LSPR) of AuNPs. The spectral peak changed to an asymmetric shape if a TiO$_2$ layer was added between the AuNPs and the quartz substrate. Typical electric field distributions at the wavelengths of the spectral peak and dip are shown in Figure 5a, the dipolar resonance of the AuNP can be observed as two lobes of plasmonic "hot spots". In light of the above comparison, it can be understood that the asymmetrical spectral peak results from the Fano resonance of the AuNPs-TiO$_2$-quartz

8

structure, i.e. the weak coupling between the thin-film interference in the titanium dioxide layer and the LSPR in the AuNPs [39-42]. According to numerical simulation, Fano asymmetric shape can be clearly observed when the TiO$_2$ layer is thicker than 40 nm (see **Figure S5a** & Figure S5b). It can be ascribed to the increased influence from the interference mode of TiO$_2$ thin-film interferometer on LSPR peak. Nevertheless, when TiO$_2$ layer is thicker than 200 nm, a few interference modes will appear around the LSPR peak (see Figure S5c & Figure S5d), which leads to a complex spectrum with varied peaks. Notably, the formation of Fano resonances in the AuNPs-TiO$_2$-quartz structure offers a new opportunity to enhance the sensing performance of AuNP-based LSPR sensors. Compared with the spectra of the AuNPs alone and the AuNPs on quartz substrate, the reflection spectra of the AuNPs-TiO$_2$-quartz structure with Fano resonance narrowed the full width at half maximum (FWHM) of the LSPR peak from 54.73 nm and 44.09 nm to 34.83 nm and increased the peak-to-valley value (PVV) from 1.58% and 6.03% to 14.12%, which are conducive to improving the performance of the LSPR sensor.

To show the potential of the AuNPs-TiO$_2$-quartz structure for label-free biosensing, the performance of the printed plasmonic substrates for refractive index sensing was tested in experiments. Figure 5c shows a comparison of the measured and simulated reflection spectra of the AuNPs-TiO$_2$-quartz structure printed with the exposure dose of 541 J/cm^2 when the surrounding reflective index (RI) is 1.334. Thereinto, the numerical simulation result has also been fitted with Breit-Wigner-Fano formula to confirm its Fano-type response. The result shows the model can also predict well the reflection spectra of the sample with bigger size of AuNPs. If compared with the reflection spectrum measured in air (i.e. when RI=1.0), one can see that the wavelength of its LSPR peak shifted significant towards longer wavelength, despite that its peak intensity was obviously reduced. The sensitivity of the printed plasmonic substrate to the change in external refractive index in the measurement range of 1.334 to 1.44 is 306.9

nm/RIU, as shown in Figure 5d, which is not far from the simulated sensitivity, i.e., 273.6 nm/RIU. Additional experiment results are shown in **Figure S6**.

In the experiments, directly printed AuNPs require thermal treatment to obtain a clear LSPR peak in the reflection spectrum, which might limit the use of precision photoreduction technology for, e.g., soft matter applications. One of the potential directions for improving the technology is further study and optimization of the additives for shape control during the growth of AuNPs. As shown in **Figure S7a**, the AuNPs printed with chloroauric acid ions and citric acid, without additional additives, show various well-crystallized structures such as hexagonal and triangular nanoparticles. However, the remarkable divergence in the geometry and size of the printed sample cannot be used to obtain a regular reflection spectrum from the printed sample. After addition of the stabilizing agent thiourea, the shape of the printed AuNPs changed dramatically, as shown in Figure S7b. The corner angles of the crystallized structures disappeared, and many tiny nanoparticles grew on the surface. Such AuNPs are especially suitable for further thermal treatment to obtain relatively uniform patterns for plasmonic applications. Further study using sophisticated additives might create new opportunities to directly print AuNPs of different shapes for various applications.

Notably, the precision photoreduction technology enables rapid micropatterning of plasmonic AuNPs without the use of expensive lithography processes. Under a UV intensity of 1803 mw/cm^2, AuNP patterns with a maximum size of 0.95 mm × 0.53 mm (as shown in Figure 2) can be printed within 180 s. This process can be scaled up to fabricate a large-area plasmonic substrate of size-controlled or size-varying AuNPs using the roll-to-roll exposure technique. Moreover, the precision photoreduction technology is a type of additive microfabrication approach in that AuNPs are precisely printed according to demand. There is no waste of gold during the fabrication processes, which is critical for such an expensive precious metal and

might render AuNP-based plasmonic substrates cost-effective and competitive in many practical applications.

In summary, we presented a precision photoreduction technology for rapid fabrication of AuNPs-based plasmonic substrates. Using a digital UV lithography setup, UV light is dynamically manipulated to precisely reduce the size-controlled AuNPs from gold(I) thiourea complex ions and form micropatterns on a TiO_2 photocatalytic layer. This process can directly and additively print micrometer-scale patterns of size-varying AuNPs for plasmonic applications. A numerical simulation was conducted to reveal that the TiO_2 layer between the AuNPs and quartz substrate leads to a Fano resonance, which can sharpen the spectral peak of LSPR and increase its peak-to-valley value. The developed precision photoreduction technology for AuNPs has the merits of high speed, scalability and material conservation, which offer new opportunities to fabricate cost-effective high-performance plasmonic substrates for various applications such as organic and biomolecules sensing, plasmonic photocatalysis, and plasmonic photothermal applications.

Experimental Section

Materials: Gold(III) chloride hydrate (~49% Au), thiourea ($\geqslant$ 99.0%), potassium sodium tartrate tetrahydrate (99%), citric acid trisodium salt dihydrate ($\geqslant$99.0%), and titanium(IV) butoxide (97%) were purchased from Sigma-Aldrich Inc. Nitric acid solution (1 mol/L aqueous solution) was purchased from Shenzhen Huashi Technology Co., Ltd. Isopropyl alcohol (IPA) was purchased from Anaqua Chemicals Supply Inc. Ltd. Quartz sheets (thickness=1 mm) were purchased from Donghai County Zhongzheng Quartz Products Factory. All materials were used as received without further purification. Deionized (DI) water with a resistance of 18 MΩ·cm was used in all experiments.

Substrate Preparation: Titanium(IV) butoxide was diluted with IPA into solutions with a mass concentration of 10%. As a hydrolysis protectant, 1 mol/L nitric acid aqueous solution was added to the solutions (volume ratio 1:100). These acidified titanium (IV) butoxide sol solutions were aged for 24 hours and used to prepare the TiO_2 layer on quartz sheets via spin-coating (400 rpm/12 s + 3000 rpm/60 s, 20 °C, 60% RH). The substrates were baked at 110 °C for 10 min to remove the solvent and to convert titanate to TiO_2 through hydrolysis. The surface morphology of the TiO_2 layer can be seen in Figure S4a. (The surface morphology of the TiO_2 layer after final thermal treatment, for reshaping AuNPs, has also been given in Figure S4b for comparison.) The thickness of TiO_2 layer is about 80 nm, as shown in Figure S4d.

Printing Processes: A gold salt solution was prepared by mixing 0.1 mol/L gold(III) chloride hydrate solution, 0.4 mol/L thiourea solution, 0.2 mol/L potassium sodium tartrate tetrahydrate solution, deionized (DI) water, and 0.2 mol/L citric acid trisodium salt dihydrate solution at a volume ratio of 1:1:1:1:4. The solution was filtered before use in experiments. Quartz substrates with the TiO_2 layer were cleaned by rinsing with IPA and blown dry with a nitrogen gun. A glass slide with a glass spacer was used to contain the gold salt solution, upon which the quartz substrate was placed upside-down to make the photocatalyst layer directly contact the gold salt solution.

An in-house digital UV lithography setup was used to expose the substrate on the gold salt solution. UV light from a 365-nm UV light-emitting diode (LED) was collimated to illuminate a digital micromirror device (DMD, DLi6500 0.65" 1080p with 1920×1080 pixels, Texas Instruments). The image data generated using 3D model slicing software were loaded to the DMD in a given time sequence to dynamically generate the predefined light patterns (256 grayscale). The maximum illumination intensity was 1803 mw/cm^2. After exposure, the quartz substrate with AuNPs was rinsed sequentially using DI water and IPA and finally dried with a

nitrogen gun. With reduction projection optics, the optical resolution (i.e., the pixel size of the light pattern) of the digital UV lithography setup was 0.493 μm.

Morphology and Optical Spectral Characterization: Color images of the samples were measured using the optical microscope module of a laser scanning confocal microscope (Keyence VK-X200 3D) and a metallurgical microscope (L3203, Guangzhou LISS Optical Instrument Co., Ltd). The samples were placed upside down on a holder, and the microscope took photographs from the top in reflection mode (i.e., taken from the AuNP layer side means that the light of the microscope illuminated the AuNP patterns and could be reflected). Electron microscope images were collected using field-emission scanning electron microscopy (TESCAN MAIA3).

The optical spectra of the samples were measured using an UV−Vis optical fiber spectrometer (USB2000+, Ocean Optics) and a metallurgical microscope (L3203, Guangzhou LISS Optical Instrument Co., Ltd). The light from the light source of microscope was collimated to illuminate the sample by a 50× objective. The reflected light was collected by the same objective and was guided to the spectrometer by an optical fiber.

Numerical Simulation: Commercial finite element method (FEM) software (COMSOL Multiphysics) was used to numerically simulate the spectral responses of the AuNP-TiO$_2$-quartz structures. The AuNPs were modeled as periodic arrays in a square lattice. A linearly polarized plane wave was assumed as the excitation light, and the structures were assumed to be illuminated at normal incidence from the side of the AuNPs. For the AuNP sample in Figure 5a and Figure 5b, the model geometric parameters are L = 98 nm, H = 56 nm, b = 35 nm; for the AuNP sample in Figure 5c, the model geometric parameters are L = 135 nm, H = 99 nm, b = 45 nm.

Supporting Information

Supporting Information is available from the Wiley Online Library or from the author.

Received: ((will be filled in by the editorial staff))
Revised: ((will be filled in by the editorial staff))
Published online: ((will be filled in by the editorial staff))

References

[1]   R. Sardar, A. M. Funston, P. Mulvaney, R. W. Murray, *Langmuir* **2009**, 25, 13840-13851. https://doi.org/10.1021/la9019475

[2]   D. A. Giljohann, D. S. eferos, W. L. Daniel, M. D. Massich, P. C. Patel, C. A. Mirkin, *Angew. Chem. Int. Ed.* **2010**, 49, 3280-3294. https://doi.org/10.1002/anie.200904359

[3]   T. R. Jensen, M. D. Malinsky, C. L. Haynes, R. P. Van Duyne, *J. Phys. Chem. B* **2000**, 104, 10549-10556. https://doi.org/10.1021/jp002435e

[4]   K. Saha, S. S.Agasti, C. Kim, X. Li, V. M. Rotello, *Chem. Rev.* **2012**, 112, 2739-2779. https://doi.org/10.1021/cr2001178

[5]   Venditti, *Materials* **2017**, 10, 97. https://doi.org/10.3390/ma10020097

[6]   M. K. Hedayati, F. Faupel, M. Elbahri, *Materials* **2014**, 7, 1221-1248. https://doi.org/10.3390/ma7021221

[7]   M. Holzinger, A. Le Goff, S. Cosnier, *Front. Chem.* **2014**, 2, 63. https://doi.org/10.3389/fchem.2014.00063

[8]   P. Ghosh, G. Han, M. De, C. K.Kim, V. M. Rotello, *Adv. Drug Deliv. Rev.* **2008**, 60, 1307-1315. https://doi.org/10.1016/j.addr.2008.03.016

[9]   X. Huang, P. K. Jain, I. H. El-Sayed, M. A. El-Sayed, *Lasers Med. Sci.* **2008**, 23, 217. https://doi.org/10.1007/s10103-007-0470-x

[10]   W. L. Leong, P. S. Lee, A. Lohani, Y. M. Lam, T. Chen, S. Zhang, A. Dodabalapur, S. G. Mhaisalkar, *Adv. Mater.* **2008**, 20, 2325-2331. https://doi.org/10.1002/adma.200702567

[11]   P. Reineck, G. P. Lee, D. Brick, M. Karg, P. Mulvaney, U. Bach, *Adv. Mater.* **2012**, 24, 4750-4755. https://doi.org/10.1002/adma.201200994

[12]   C. Gomes Silva, R. Juárez, T. Marino, R. Molinari, H. García, *J. Am. Chem. Soc.* **2010**, 133, 595-602. https://doi.org/10.1021/ja1086358

[13]   D. S. Indrasekara, S. Meyers, S. Shubeita, L. C. Feldman, T. Gustafsson, L. Fabris, *Nanoscale* **2014**, 6, 8891-8899. https://doi.org/10.1039/C4NR02513J

[14]   S. E. Skrabalak, J. Chen, Y. Sun, X. Lu, L. Au, C. M. Cobley, Y. Xia, *Acc.* **2008**, 41, 1587-1595. https://doi.org/10.1021/ar800018v

[15]   M. R. Langille, M. L. Personick, J. Zhang, C. A. Mirkin, *J. Am. Chem. Soc.* **2012**, 134, 14542-14554. https://doi.org/10.1021/ja305245g

[16]   P. H. N. Diem, D. T. T. Thao, D. V. Phu, N. N. Duy, H. T. D. Quy, T. T. Hoa, N. Q. Hien, *J. Chem.* **2017**, 2017. https://doi.org/10.1155/2017/6836375

[17]   P. R. Teixeira, M. S. Santos, A. L. G.Silva, S. N. Báo, R. B. Azevedo, M. J. A. Sales, L. G. Paterno, *Colloids Surf. B* **2016**, 148, 317-323. https://doi.org/10.1016/j.colsurfb.2016.09.002

[18]   M. Annadhasan, J. Kasthuri, N. Rajendiran, *RSC Adv.* **2015**, 5, 11458-11468. https://doi.org/10.1039/C4RA14034F

[19]   K. Okitsu, K. Sharyo, R. Nishimura, *Langmuir* **2009**, 25, 7786-7790.

https://doi.org/10.1021/la9017739

[20]   V. Kabashin, M. Meunier, *J. Appl. Phys.* **2003**, 94, 7941-7943.

https://doi.org/10.1063/1.1626793

[21]   K. Maximova, A. Aristov, M. Sentis, A. V. Kabashin, *Nanotechnology* **2015**, 26,

065601. https://doi.org/10.1088/0957-4484/26/6/065601

[22]   S. Ahmed, S.Ikram, Photobiol. *B, Biol.* **2016**, 161, 141-153.

https://doi.org/10.1016/j.jphotobiol.2016.04.034

[23]   M. Kitching, M. Ramani, E. Marsili, *Microb. Biotechnol.* **2015**, 8, 904-917.

https://doi.org/10.1111/1751-7915.12151

[24]   E. P. Hoppmann, W. Y. Wei, I. M. White, *Methods* **2013**, 63, 219-224.

https://doi.org/10.1016/j.ymeth.2013.07.010

[25]   Q. Li, J. He, E. Glogowski, X. Li, J. Wang, T. Emrick, T. P. Russell, *Adv. Mater.*

2008, 20, 1462-1466. https://doi.org/10.1002/adma.200702004

[26]   V. Santhanam, R. P.Andres, *Nano Lett.* **2004**, 4, 41-44.

https://doi.org/10.1021/nl034851r

[27]   J. Henzie, M. H. Lee, T. W. Odom, *Nat. Nanotechnol.* **2007**, 2, 549.

https://doi.org/10.1038/nnano.2007.252

[28]   K. Kumar, H. Duan, R. S. Hegde, S. C. Koh, J. N. Wei, J. K. Yang, *Nat. Nanotechnol.*

2012, 7, 557. https://doi.org/10.1038/nnano.2012.128

[29]   V. G. Kravets, F. Schedin, R. Jalil, L. Britnell, R. V. Gorbachev, D. Ansell, B.

Thackray, K. S. Novoselov, A. K. Geim, A. V. Kabashin, A. N. Grigorenko, *Nat. Mater.*

2013, 12, 304-309. https://doi.org/10.1038/nmat3537

[30]   J. M. Guay, A. C. Lesina, G. Côté, M. Charron, D. Poitras, L. Ramunno, P. Berini, A.

Weck, *Nat. Commun.* **2017**, 8, 1-12. https://doi.org/10.1038/ncomms16095

[31]   Q. C. Tong, M. H. Luong, J. Remmel, M. T. Do, D. T. T. Nguyen, N. D. Lai, *Opt. Lett.* **2017**, 42, 2382-2385. https://doi.org/10.1364/OL.42.002382

[32]   T. Hezard, K. Fajerwerg, D. Evrard, V. Collière, P. Behra, P. Gros, *J. Electroanal. Chem.* **2012**, 664, 46-52. https://doi.org/10.1016/j.jelechem.2011.10.014

[33]   G. Pető, G. L. Molnar, Z. Paszti, O. Geszti, A. Beck, L.Guczi, *Mater. Sci. Eng.* **2002**, 19, 95-99. https://doi.org/10.1016/S0928-4931(01)00449-0

[34]   A. Schaub, P. Slepička, I. Kašpárková, P. Malinský, A. Macková, V. Švorčík, *Nanoscale Res. Lett.* **2013**, 8, 1-8. https://doi.org/10.1186/1556-276X-8-249

[35]   Y. Zhang, Q. Zhang, X. Ouyang, D. Y. Lei, A. P. Zhang, H. Y. Tam, *ACS nano* **2018**, 12, 9913-9921. https://doi.org/10.1021/acsnano.8b02868

[36]   M. H. Magnusson, K. Deppert, J. O. Malm, J. O. Bovin, L. Samuelson, *J. Nanopart. Res.* **1999**, 1, 243-251. https://doi.org/10.1023/A:1010012802415

[37]   B. Taylor, A. M. Siddiquee, J. W.Chon, *ACS nano* **2014**, 8, 12071-12079. https://doi.org/10.1021/nn5055283

[38]   Freestone, N. Meeks, M. Sax, C. Higgitt, *Gold Bull.* **2007**, 40, 270-277. https://doi.org/10.1007/BF03215599

[39]   M. F. Limonov, M. V. Rybin, A. N. Poddubny, Y. S.Kivshar, *Nat. Photonics* **2017**, 11, 543-554. https://doi.org/10.1038/nphoton.2017.142

[40]   B. Gallinet, O. J. Martin, *Phys. Rev. B* **2011**, 83, 235427. https://doi.org/10.1103/PhysRevB.83.235427

[41]   B. Gallinet, O. J. Martin, *ACS nano* **2011**, 5, 8999-9008. https://doi.org/10.1021/nn203173r

[42]   Y. S. Joe, A. M. Satanin, C. S. Kim, *Phys. Scr.* **2006**, 74, 259. https://doi.org/10.1088/0031-8949/74/2/020
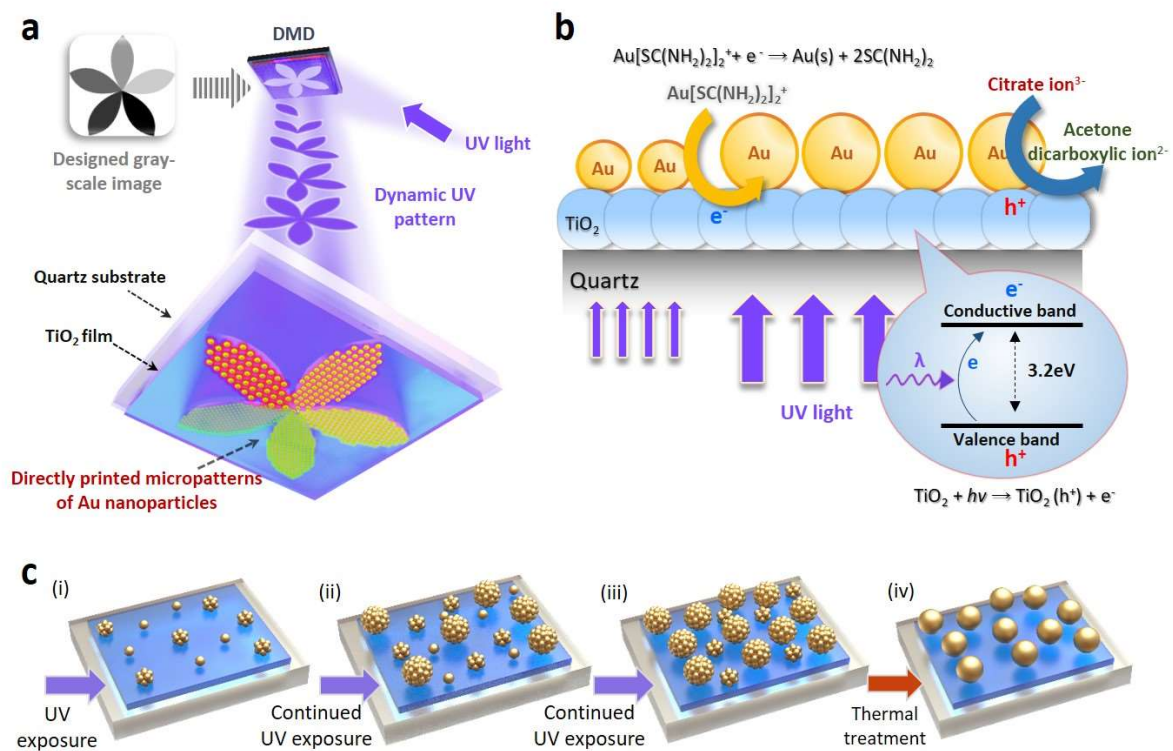
Figure 1. Schematic diagrams for direct micropattern printing of size-controlled AuNPs. a) Mask-less ultraviolet exposure technology for precision photoreduction; b) light-controlled growth of AuNPs on the photocatalyst layer; c) process flow for light-controlled growth and thermal reshaping of AuNPs.
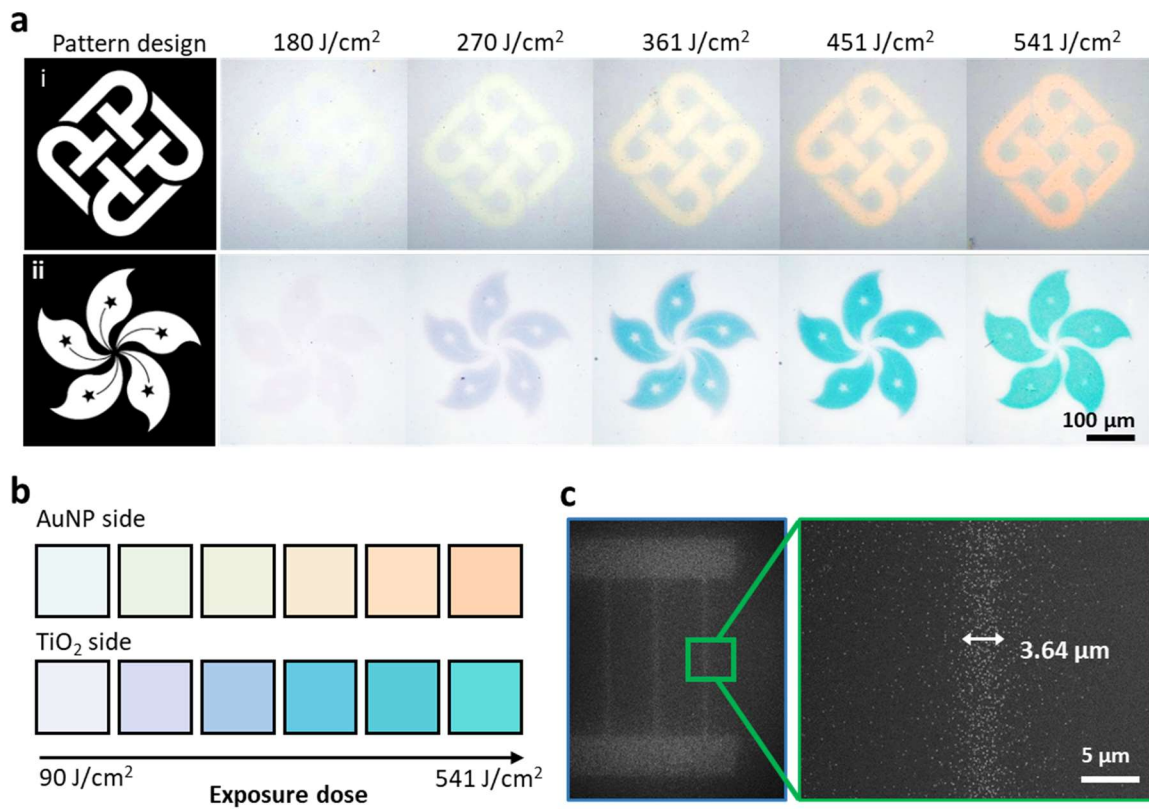
Figure 2. Micropatterns and colors of AuNPs printed on TiO₂-capped quartz substrate. a) Optical reflection-mode microscopy images of AuNP micropatterns printed with different exposure doses: i. Images viewed from AuNP side; ii. Image viewed from TiO₂–layer side. b) Collections of the colors of printed micropatterns; c) SEM images of the printed AuNP micropattern with 3.64-µm-wide lines.
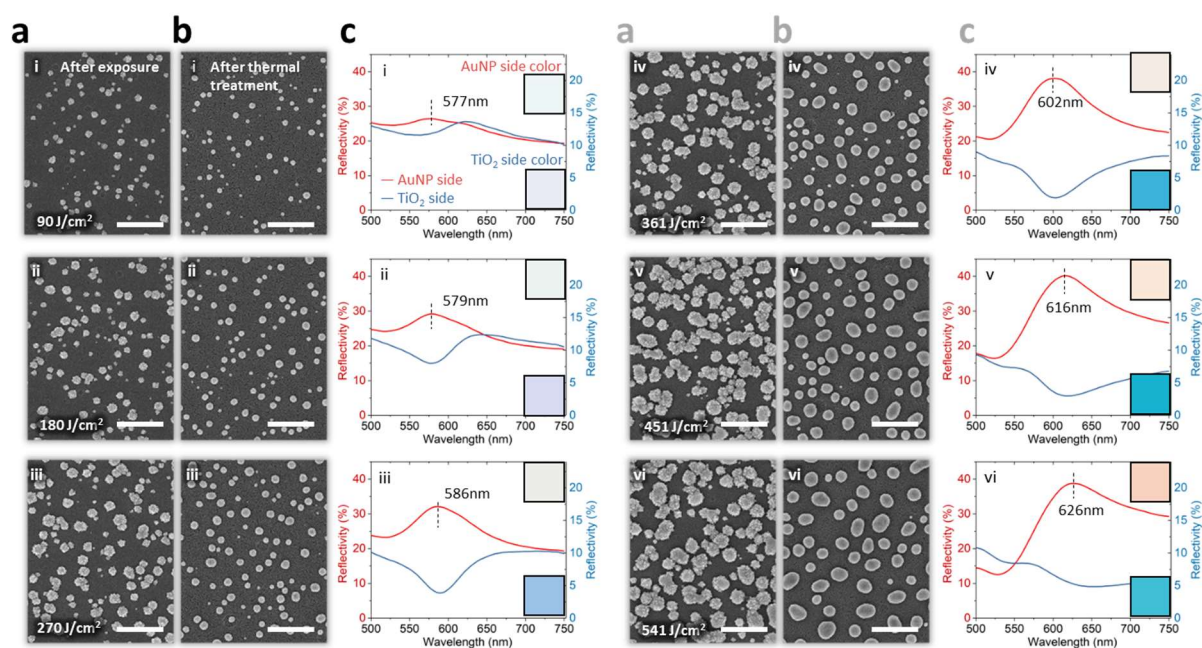
Figure 3. SEM images of printed AuNPs and reflection spectra of the corresponding plasmonic substrates. a) SEM image of directly printed AuNPs before thermal treatment, scale bar represents 500 nm; b) SEM image of printed AuNPs after thermal treatment, scale bar represents 500 nm; c) reflection spectra of fabricated plasmonic substrates. Red curves and blue curves show the spectra measured from the AuNP side and TiO_2-layer side, respectively. The upper-right and bottom-right insets present the corresponding colors observed from the AuNP side and TiO_2-layer side, respectively.
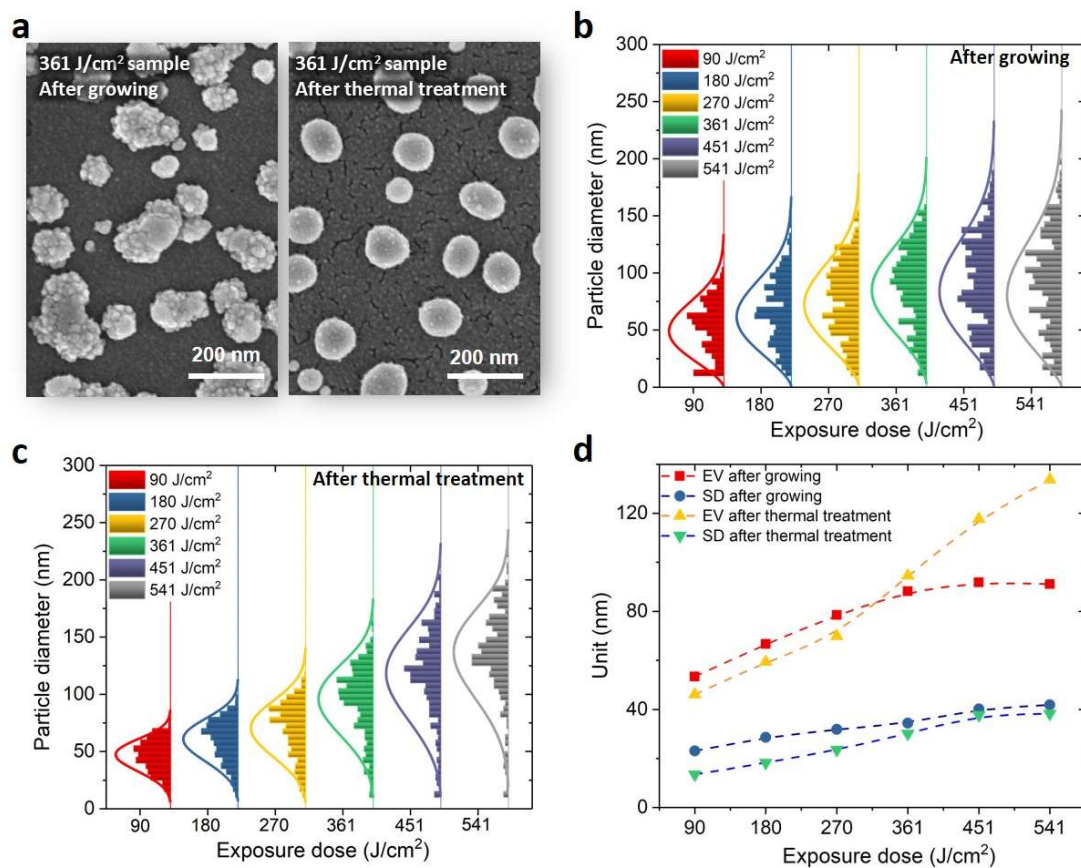
Figure 4. Comparison of AuNP morphology before and after thermal treatment. a) SEM images of AuNPs before and after thermal treatment. The exposure dose is 361 J/cm^2. b) Size distributions of AuNPs printed with different exposure doses. c) Size distributions of AuNPs after thermal treatment. d) Expected value and standard deviation of the diameter of AuNPs before and after thermal treatment.
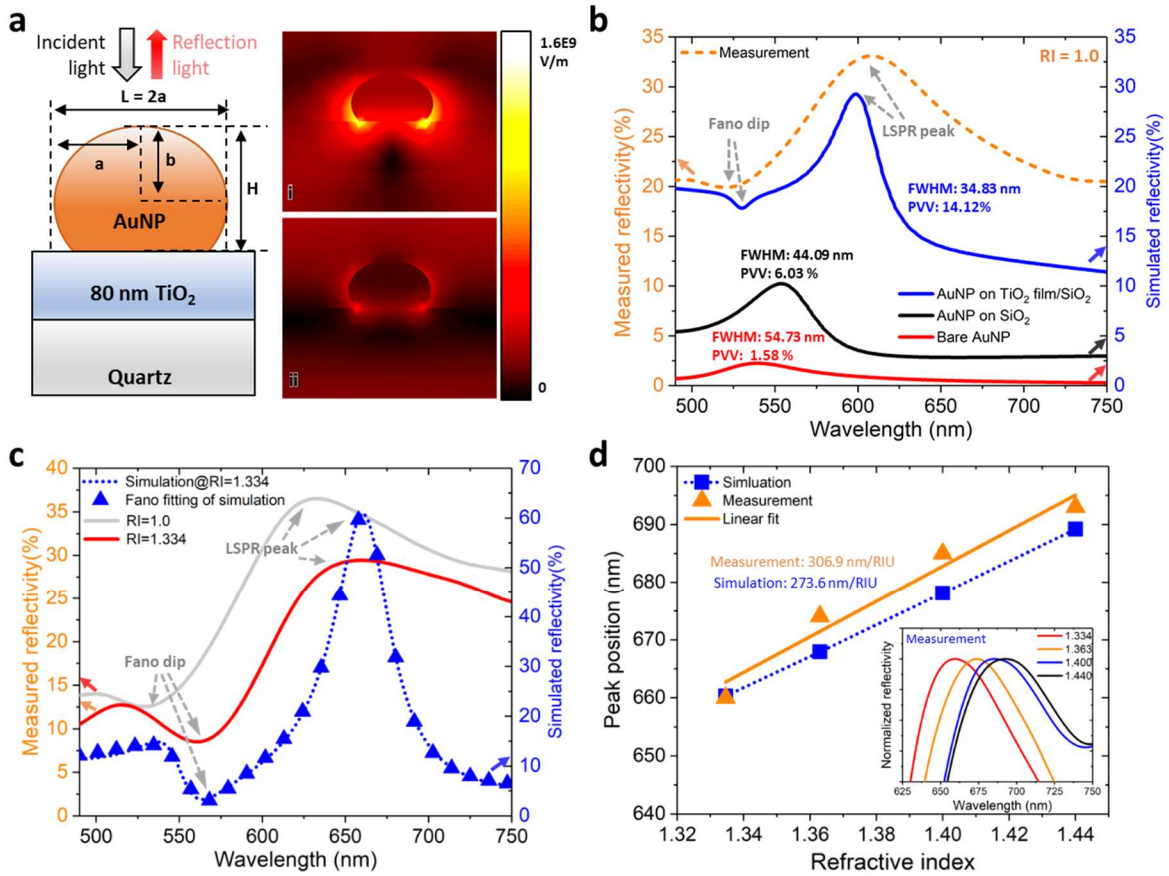
Figure 5. Numerical simulation of the reflection spectra of the AuNPs-TiO$_2$-quartz structure and comparison with experiment results. a) Simulation model and the simulated local electric fields at the wavelengths of the LSPR peak (i) and Fano dip (ii), respectively. b) Comparison of the measured reflection spectra of a printed structure with the simulated reflection spectra. The simulated reflection spectra of the same AuNPs upon quartz substrate and even without substrate are also presented for comparison. c) Measured and simulated reflection spectra of an AuNPs-TiO$_2$-quartz structure when its external refractive index is 1.334. The measured spectrum of the structure in air is also given for comparison. d) Measured and simulated spectral responses of the AuNPs-TiO$_2$-quartz structure to the change of external reflective index.

Table of contents

Keywords: plasmonic substrate, gold nanoparticle, optical printing, precision photoreduction

Yangxi Zhang[1], Zengtian Liang[1], A. Ping Zhang[1*] and Hwa-Yaw Tam[1]

Direct Printing of Micropatterned Plasmonic Substrates of Size-controlled Gold Nanoparticles by Precision Photoreduction
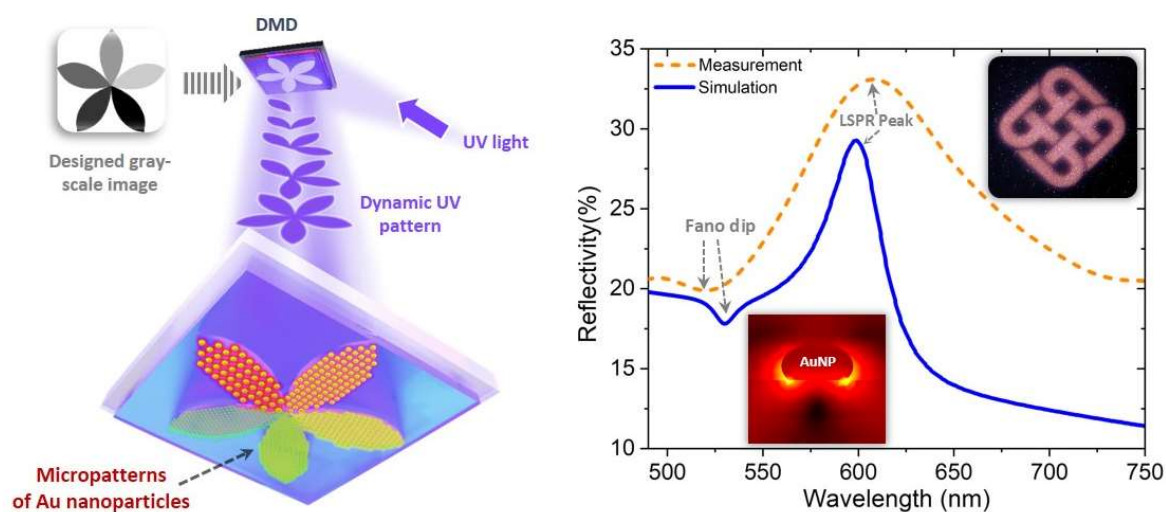
We present a method for the direct printing of micropatterns of size-controlled gold nanoparticles (AuNPs). A precision photoreduction technology is developed for light-controlled growth of AuNPs to create micrometer-scale micropatterns on a titanium dioxide photocatalytic layer. This printing technology offers new opportunities to develop various miniature plasmonic devices ranging from plasmonic biosensors to plasmonically enhanced photothermal and photovoltaic applications.

Supporting Information

Direct Printing of Micropatterned Plasmonic Substrates of Size-controlled Gold Nanoparticles by Precision Photoreduction

Yangxi Zhang[1], Zengtian Liang[1], A. Ping Zhang[1*] and Hwa-Yaw Tam[1]

[1]Photonics Research Center, Department of Electrical Engineering, The Hong Kong Polytechnic University, Hung Hom, Hong Kong SAR, China

[*]Email address: azhang@polyu.edu.hk
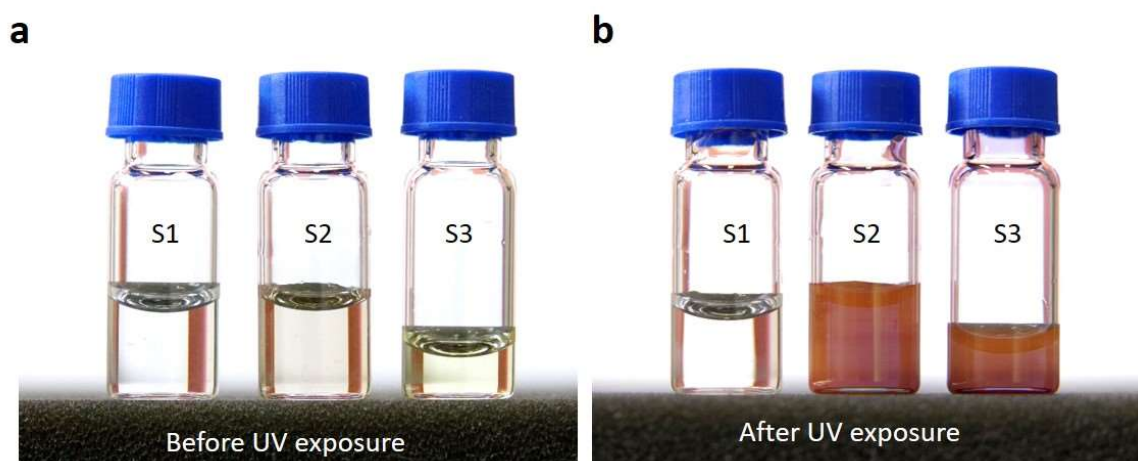
Figure S1. Comparison of three precursor solutions before and after UV irradiation. Sample S1: Precursor solution with gold(I) thiourea complex ion; Sample S2: Mixed solution of tetrachloride gold (III) and sodium citrate at the same concentration; Sample S3: Mixed solution of tetrachloride gold (III), potassium sodium tartrate and sodium citrate at the same concentration. a) mixed solution before UV irradiation; b) Mixed solution after 365-nm UV irradiation under 250 J/cm^2.
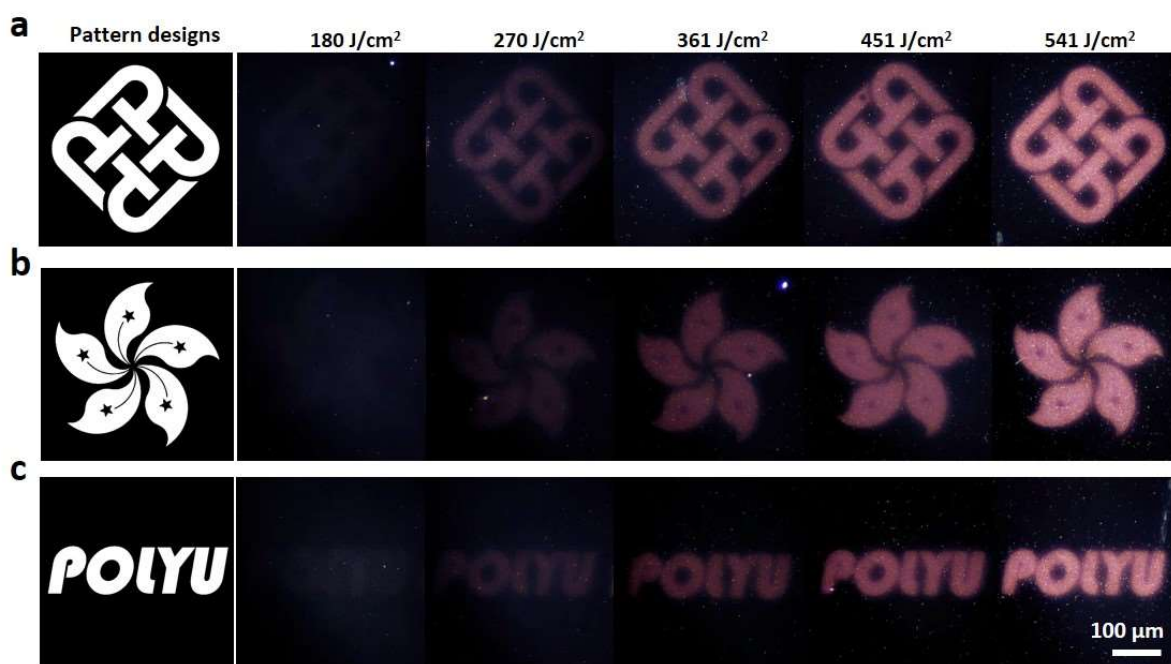
Figure S2. Dark-field microscopy images of the micropatterns of gold nanoparticles printed with different exposure dose using different images: a) the university logo; b) Hong Kong bauhinia; c) the abbreviation of university name.

a

5.9 µm

10 µm

b

10 µm
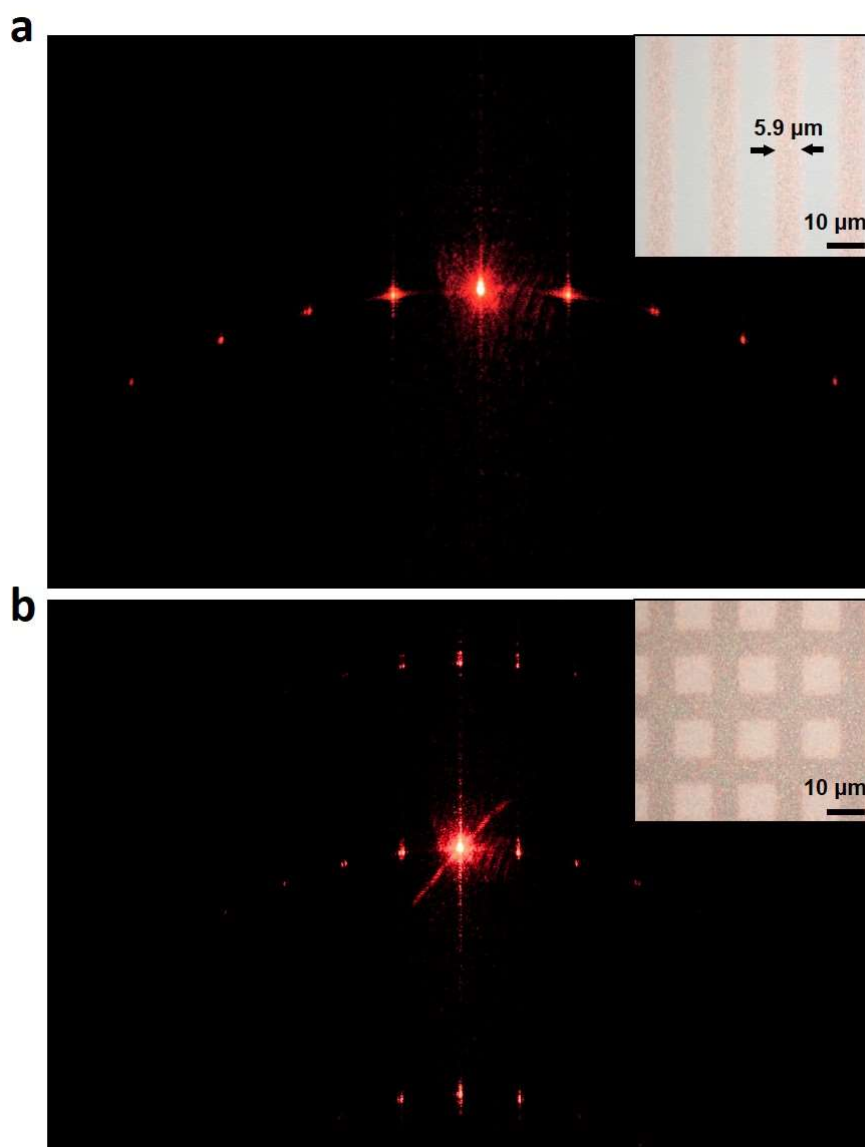
Figure S3. Reflected optical diffraction patterns of a light from 633-nm laser after tilted incident on the substrate with printed gratings of gold nanoparticles: a) 1D grating; b) 2D grating.
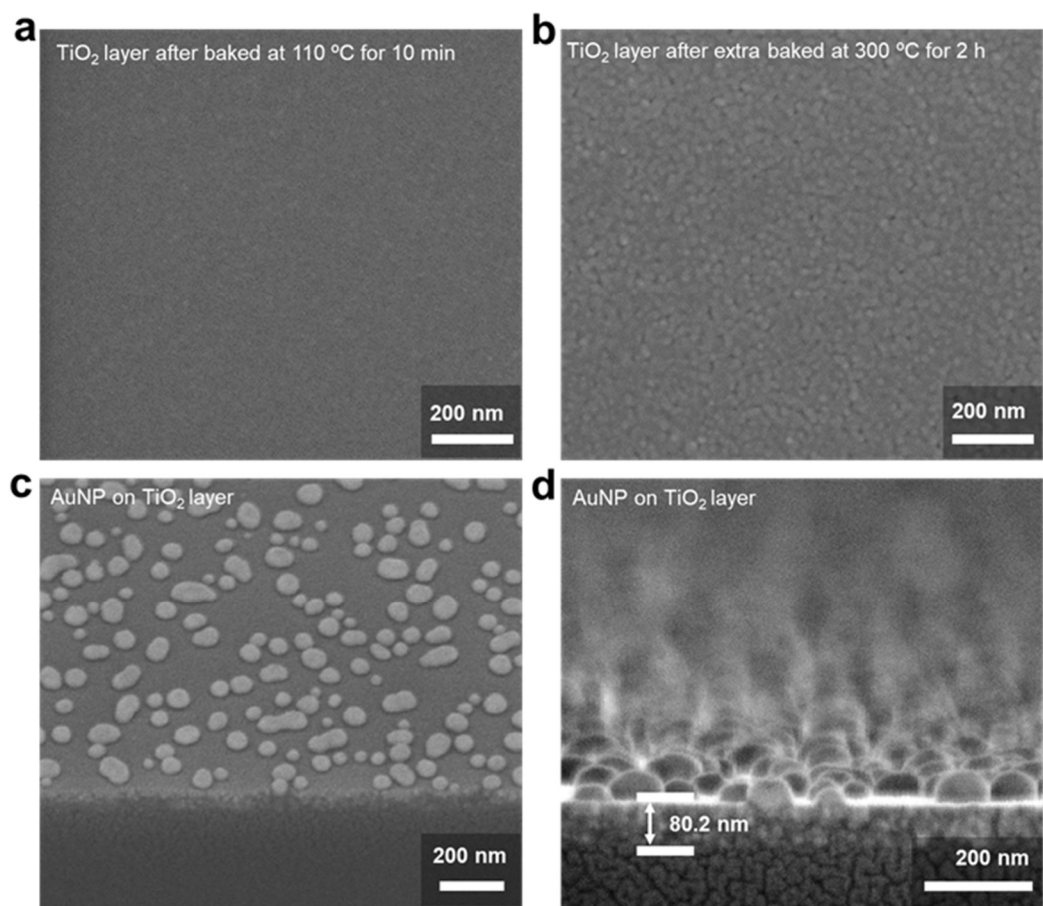
Figure S4. High-magnification SEM images of TiO$_2$ layer and AuNPs. a) TiO$_2$ layer baked at 110 °C for 10 min. b) TiO$_2$ layer after final thermal treatment at 300 °C for 2 h. c) Cross-sectional view (about 45°) of AuNPs printed on TiO$_2$ layer after thermal treatment. d) Cross-sectional view (about 90°) of AuNPs printed on TiO$_2$ layer after thermal treatment.
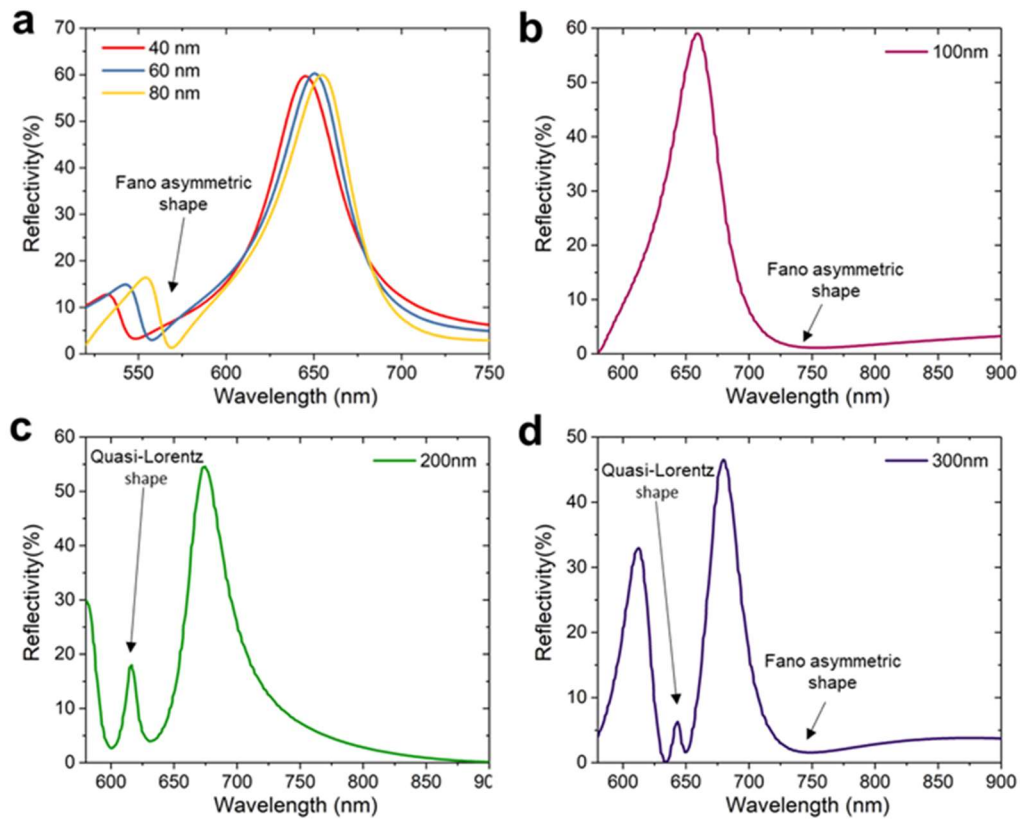
Figure S5. Simulated reflection spectra of plasmonic AuNPs-TiO$_2$ film structures. a) The thickness of TiO$_2$ layer is 40 ~ 80 nm. b-d) The thickness of TiO$_2$ layer is 100, 200, and 300 nm, respectively. The size parameters of AuNPs used in the simulation are L = 135 nm, H = 99 nm, b = 45 nm.
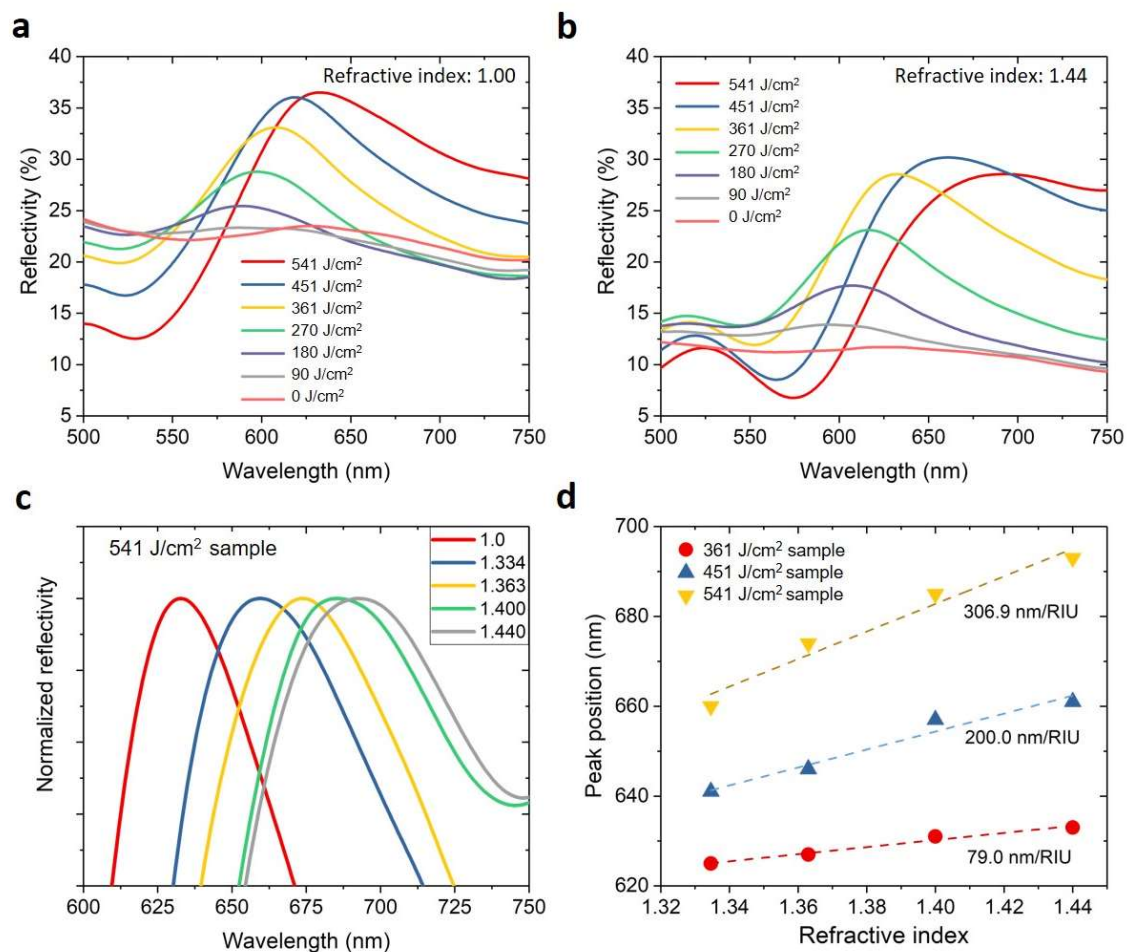
Figure S6. Experiment result of the printed substrate of AuNPs (whose exposure dose is 0~541 J/cm^2) for plasmonic reflective index sensing . a) The reflectance spectra in air (Refractive index 1.0). b) The reflectance spectra in the standard refractive-index liquid with the refractive index 1.44. c) Normalized LSPR peaks at different refractive indices (sample with exposure dose 541 J/cm^2). d) Comparison of simulated reflective index sensitivity with different exposure dose.
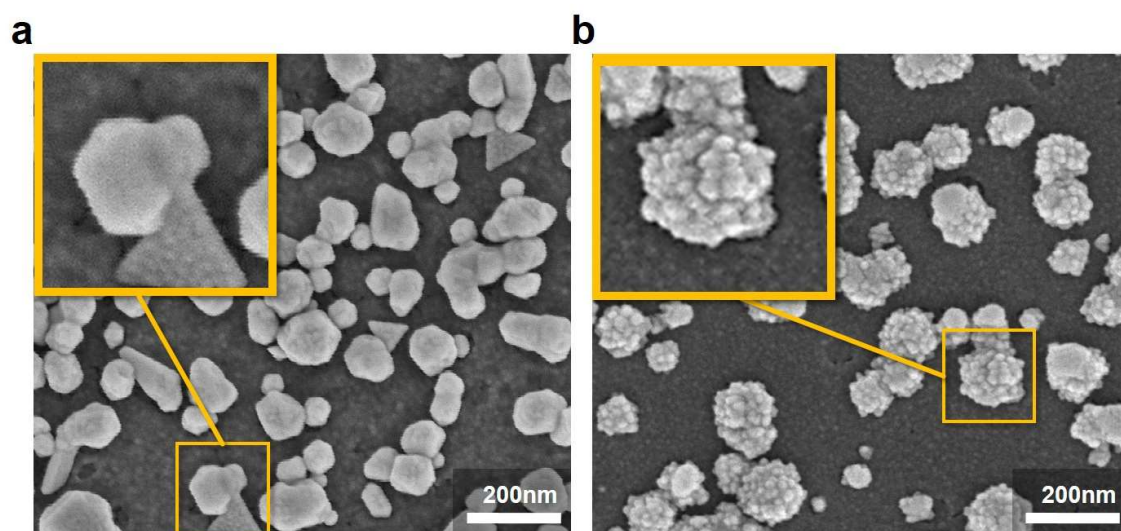
Figure S7. The influence of thiourea as additive agent on the morphology of AuNPs. a) AuNPs photoreduced with only citric acid; b) AuNPs photoreduced with citric acid and thiourea.